J Nanopart Res (2011) 13:2049–2062
DOI 10.1007/s11051-010-9959-5

RESEARCH PAPER

NMR-based metabonomic analyses of the effects of ultrasmall superparamagnetic particles of iron oxide (USPIO) on macrophage metabolism

Jianghua Feng · Jing Zhao · Fuhua Hao · Chang Chen · Kishore Bhakoo · Huiru Tang

Received: 15 June 2009 / Accepted: 8 May 2010 / Published online: 26 May 2010

Abstract The metabonomic changes in murine RAW264.7 macrophage-like cell line induced by ultrasmall superparamagnetic particles of iron oxides (USPIO) have been investigated, by analyzing both the cells and culture media, using high-resolution NMR in conjunction with multivariate statistical methods. Upon treatment with USPIO, macrophage cells showed a significant decrease in the levels of triglycerides, essential amino acids such as valine, isoleucine, and choline metabolites together with an increase of glycerophospholipids, tyrosine, phenylalanine, lysine, glycine, and glutamate. Such cellular responses to USPIO were also detectable in compositional changes of cell media, showing an obvious depletion of the primary nutrition molecules, such as glucose and amino acids and the production of end-products of glycolysis, such as pyruvate, acetate, and lactate and intermediates of TCA cycle such as succinate and citrate. At 48 h treatment, there was a differential response to incubation with USPIO in both cell metabonome and medium components, indicating that USPIO are phagocytosed and released by macrophages. Furthermore, information on cell membrane modification can be derived from the changes in choline-like metabolites. These results not only suggest that NMR-based metabonomic methods have sufficient sensitivity to identify the metabolic consequences of murine RAW264.7 macrophage-like cell line response to USPIO in vitro, but also provide useful information on the effects of USPIO on cellular metabolism.

Keywords Metabonomics · USPIO · NMR spectroscopy · Macrophage · Nanobiology · Nanomedicine

J. Feng · F. Hao · H. Tang (✉)
State Key Laboratory of Magnetic Resonance and Atomic and Molecular Physics, Wuhan Institute of Physics and Mathematics, The Chinese Academy of Sciences, Wuhan 430071, China
e-mail: huiru.tang@wipm.ac.cn

J. Zhao · C. Chen
National Laboratory of Biomacromolecules, Institute of Biophysics, The Chinese Academy of Sciences, Beijing, China

K. Bhakoo
Singapore Bioimaging Consortium Agency for Science, Technology and Research (A*STAR), Singapore, Singapore

Present Address:
J. Zhao
China Institute of Atomic Energy, Beijing, China

Introduction

Ultrasmall superparamagnetic particles of iron oxides (USPIO) have been developed as intravenous contrast agents in magnetic resonance imaging (MRI) for the lymphatic system (Anzai et al. 2003; Saksena et al. 2006), bone marrow (Daldrup-Link et al. 2003; Metz

et al. 2006), central nervous system (CNS) (Dousset et al. 1999; Fabene et al. 2003), and the magnetic moiety in organ-targeted superparamagnetic contrast agent (Weishaupt et al. 2000; Halbreich et al. 2002).

As an MRI contrast agent, the USPIO is small enough to be employed intravenously and can be phagocytosed by monocytes (Metz et al. 2004). Following intravenous administration, the USPIO can be cleared effectively from the blood (Pouliquen et al. 1991) through specific internalization (Pouliquen et al. 1991; Weissleder et al. 1997; Metz et al. 2004; Kresse et al. 2005) and phagocytosis (Saini et al. 1987; Dousset et al. 1999) by the cells of the reticuloendothelial system (RES) such as macrophages in liver and spleen. Some USPIO products are currently being evaluated in phase II and III trials for clinical applications (Anzai et al. 2003) as markers for lymph node and bone marrow due to the pathologic regions possessing an aberrant phagocytic activity.

Dextran-coated USPIO is biocompatible (Shen et al. 1993; Bulte et al. 1993) and easily phagocytosed by monocytes and/or macrophages (LaConte et al. 2005). Macrophages are considered important effector cells and play a major role in many pathophysiologic processes. However, the effects of magnetic nanoparticle probes on the biochemistry of macrophage cells remain largely unknown. Furthermore, different target cells can also affect the intracellular localization of such nanoparticles. Over the last decade, most work in developing magnetic nanoparticles for biomedical and biochemistry fields has been based on either particle-size-dependent tissue accumulation or targeting extracellular components to achieve specificity; however, much less research was performed on intracellular molecular biochemical processes to assess the potential of this new class of nanoprobes.

Understanding the effects of USPIO on cellular metabolism is a good starting point and such investigation can be performed in the systemic level with metabonomics approach. With the capability of obtaining holistic metabolic information on the responses of biological systems to both endogenous and exogenous factors (Nicholson et al. 1999; Tang and Wang 2006), the metabonomics approaches have already found widespread successful applications in understanding the metabolic aspects of carcinogenesis (Yang et al. 2007), toxicological effects (Wei et al. 2009), stresses (Wang et al. 2006), parasitic disease (Wang et al. 2004; Li et al. 2009), and environmental sciences (Bundy et al. 2002; Simpson and McKelvie 2009). Such approach is powerful in detecting significant metabolite changes (e.g., in NMR spectra) in response to a treatment. In particular, the introduction of high-resolution magic-angle-spinning (HRMAS)-NMR spectroscopy has made it possible to investigate intact tissues (Bollard et al. 2000; Coen et al. 2004; Wang et al. 2005, 2007, 2008) and cells *ex vivo*, which avoids sample destruction, thus providing detailed information about their biochemical processes.

Recently, metabonomics approaches have also been used for cellular systems including both intact cells and media (Griffin et al. 2002, 2003; Duarte et al. 2009; Lamers et al. 2003), which provides a simple model that is best used for studying the basic mechanisms of pathophysiological processes and pharmacological responses (Yang et al. 2005). Metabonomics using in vitro models appears to be a feasible technique that allows the characterization of metabolic response and biochemical process of cells under controlled conditions. Compared with in vivo models, such in vitro models offer further advantages, such as its relative inexpensive and quick processing, reducing the heavy workload and complexity of whole animal studies.

In this study, we investigated the effects of USPIO on the metabonome of murine RAW264.7 macrophage-like cell line by analyzing both their culture media and intracellular metabolism using high-resolution NMR spectroscopy and multivariate statistics. The overall objective of this study was to understand the dosage and dynamic effects of USPIO on the endogenous metabolism of cells.

Materials and methods

Ultrasmall superparamagnetic particles of iron oxides

Dextran-coated iron oxide nanoparticles (IODEX) were prepared in-house as reported previously (Josephson et al. 1999). The USPIO is composed of an iron oxide core covered with a biocompatible hydrophilic dextran coat. The diameter of iron oxide core varies from 2.3 to 4.0 nm, and the corresponding hydrated particle diameter is 20 ± 2 nm. Owing to its size, it cannot diffuse easily out of the vascular space and is principally cleared from blood by macrophages. The iron concentration in USPIO was

determined by Inductively Coupled Plasma-Atomic Emission Spectrometry (ICP-AES). Cells were incubated with USPIO at a number of varying concentrations ranging from 0.5 to 5 μmol iron/10^7 cells.

In vitro experiment

Murine macrophage cell lines (RAW264.7) were obtained from Peking Union Medical College (Beijing, China) and activated with lipopolysaccharide (LPS).

The culture media consisted of DMEM (Delbecco's Modified Eagle Medium) supplemented with 10% heat-inactivated fetal calf serum (FCS). Cell cultures were maintained at 37°C with 5% CO_2. Fresh stock of macrophage cells were seeded at a density of 1.0×10^5 cells/25 cm^2 flask in seven identical sets (five samples each). After 2 days, the growth medium was replaced with fresh growth medium and the cells were allowed to grow further for another 2 days during which the cells became confluent (approximately 10^7 cells/flask). At 100% confluence, the cells were fed with various media. The cells from each flask of the three sets were treated with 10 μL USPIO solution (5 mM; low dosage), and another three sets were treated with 100 μL USPIO solution (50 mM; high dosage), while the other flasks served as the control. The control set (0 h samples) was collected directly after the start of the exposure. The cells in the remaining six sets of flasks were incubated for either 6, 24, or 48 h, after which, two sets of flasks (both low dosage and high dosage) were harvested by trypsinization with 1 mL trypsin solution. All macrophages in trypsin solution were centrifuged at 1000 g for 5 min. The supernatants were discarded, and the cells were washed twice with ice-cold PBS (4 °C, pH = 7.4). The macrophages collected were immediately snap frozen in liquid nitrogen and stored at −80 °C until NMR analysis.

In addition, 1.5 mL of cell culture medium was collected before harvesting cells and cleared by centrifugation (10 min, 12000*g*). The supernatants were stored at −80 °C until ^{1}H-NMR experiments were performed for analyzing the extracellular metabolites from the medium.

Cell conditions at the different time points were monitored by Trypan blue staining and microscopic method. No obvious cell death was found during cell incubation. With a maximal iron oxide uptake of up to 50 pg Fe/cell by monocytes without impairment of cell viability (Metz et al. 2004), cell lysis will only be a minor effect in our experiments.

NMR experiments

^{1}H-high-resolution magic-angle-spinning NMR spectroscopy

The macrophages pellets (approximately 20 mg) were packed into separate 4 mm-diameter zirconium oxide rotors with sufficient saline in D_2O added to maintain a cellular osmolality and to provide a field lock. All the HRMAS ^{1}H-NMR spectra were recorded at 298 K on a Varian INOVA-600 NMR spectrometer equipped with a Varian nanoprobe, operating at a ^{1}H frequency of 599.90 MHz. Cell samples were spun at 2 kHz (due to hardware-imposed speed restriction) at the magic angle. A total of 15 min was allowed for the temperature equilibration before NMR acquisition. A standard one-dimensional ^{1}H-NMR spectrum was acquired to obtain all observed metabolites signals using a NOESYPR1D pulse sequence (recycle delay-90-t_1-90-t_m-90-acquisition), where t_1 delay was 3 μs and the mixing time t_m was 100 ms. Typically, 128 transients were acquired with 32 k data points with the water signal irradiated during the recycle delay and mixing time. The 90° pulse length was adjusted to 9.6 to 10 μs individually for each sample. A spectral width of 20 ppm and an acquisition time of 2.73 s were used for the data acquisition. For assignment purpose, 2D ^{1}H-^{1}H total correlation spectroscopy (TOCSY) spectra were recorded on selected samples with the mixing time of 50 ms, 2 k data points, and 16 transients for each of the 256 increments.

^{1}H-NMR spectroscopy of cell culture medium

NMR measurements of cell culture medium were carried out at 298 K in random order and in triplicate in a fully automated manner on a Bruker AVIII 600 MHz spectrometer (Bruker BioSpin GmbH, Rheinstetten, Germany) equipped with an inverse cryogenic probe. For each sample, the standard NOESYPR1D pulse sequence was employed with the irradiations at the water frequency during the recycle delay of 2 s and the mixing time of 100 ms to suppress the water signal. 90° pulse length was adjusted to about 10 μs for each sample; t_1 was set to

3 μs; 64 transients were acquired at 32 k data points with a spectral width of 20 ppm.

Standard COSY, TOCSY, and J-resolved spectra were also acquired for the metabolite identification purpose for the selected cell culture medium sample.

Multivariate data analysis

The NMR data for cells were converted into Bruker format. For all 1D ^{1}H-NMR spectra, free induction decays (FIDs) were multiplied by an exponential function with a line-broadening factor of 1.0 Hz prior to Fourier transformation and were manually phased and baseline-corrected using Topspin 2.0 software. The spectra were referenced to the anomeric proton resonance of α-glucose resonance at δ5.223. The spectral region δ9.0–0.5 was automatically divided into integral segments of equal width (0.005 ppm) using AMIX (v3.8, Bruker Biospin). In the case of HRMAS NMR spectra, the regions of δ8.77–8.55, δ5.27–5.20, δ4.90–4.66, and δ4.37–4.21 were removed to eliminate the effects of imperfect water suppression and sidebands. For the cell medium, the ^{1}H-NMR spectra (δ9.0–0.5) were divided into regions with equal width of 0.005 ppm using AMIX after phase and baseline corrections. The spectra were referenced to the lactate methyl resonance at δ1.33. The regions of δ6.88–5.27 and δ5.21–4.28, δ3.875–3.81, and δ3.20–2.67 were excluded to eliminate the residual water and HEPES signals, respectively. After normalization of the spectra to the total integration value for each spectrum, principal component analysis (PCA) and orthogonal projection to latent structure with discriminant analysis (OPLS-DA) and projection to latent structure with discriminant analysis (PLS-DA) were carried out with the software package SIMCA-P + (v11.0, Umetrics, Sweden). PCA was performed using mean-centered data, and the data were visualized in the form of the PC scores plots where each point represented an individual sample. OPLS-DA was carried out using unit variance scaling (UV), the loading in the coefficient plots were calculated back from the coefficients incorporating the weight of the variables contributing to the sample classification in the model. The coefficient plots were generated with MATLAB scripts (downloaded from http://www.mathworks.com) with some in-house modifications and were color-coded with absolute value of coefficients (r). The coefficient plots provide information on spectral regions responsible for the classification of samples and the significance of such contribution. In our study, a correlation coefficient of $|r| > 0.811$ was used as the cutoff value for the statistical significance based on the discrimination significance at the level of $p < 0.05$, which was determined according to the test for the significance of the Pearson's product-moment correlation coefficient.

Results and discussions

Cellular metabolism is a set of chemical reactions, required for cellular maintenance and function, which often changes in response to environmental factors or stimuli. Thus, information can be obtained for the metabolic pathways and biochemical processes of the macrophages at a given time point by observing changes of metabolites in these cells. Since cells are sensitive to availability of nutritional substrates, the metabolites compositional changes in culture medium reflect not only the substrate utilization and production but also the physiological state and phenotype of the cells; thus these variables are reported as the cellular metabonome (Kell et al. 2005).

Metabolite profiles of macrophages and composition changes of culture media

HRMAS ^{1}H-NMR spectra were acquired from USPIO treated macrophages in order to observe the effects of the nanoparticles on their metabolic profiles. Primary resonances in the ^{1}H-NMR spectra of macrophages were assigned to individual metabolites according to the literature (Akhtar et al. 2007; Lamers et al. 2003; Bundy et al. 2006), in-house NMR database and further confirmed with analysis of the 2D ^{1}H-^{1}H TOCSY spectra. Figure 1 shows HRMAS ^{1}H-NMR spectra of macrophages from pre- and 24 h post-treatment groups with low-dosage USPIO, and assigned metabolites are labeled directly on the spectra. The cell spectra profiles were characterized by the predominance of various lipids and choline metabolites, together with resonances from phosphocreatine, several amino acids, and organic acids.

Figure 2 shows the ^{1}H-NMR spectra of cell growth media following the treatments of USPIO,

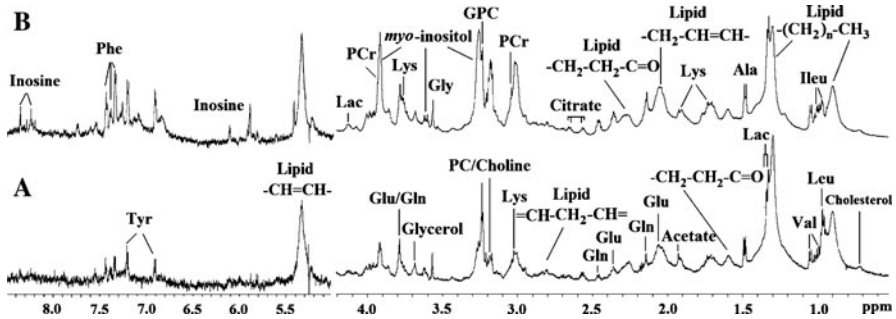

Fig. 1 Representative 600 MHz ^{1}H-MAS NMR spectra (δ0.5–4.2, δ5.0–8.5) of macrophages **a** pre- and **b** 24 h post-treatment with low-dosage USPIO. The aromatic region was magnified four times compared with corresponding aliphatic region for the purpose of clarity. Key: *Ala* Alanine, *Gln* Glutamine, *Glu* Glutamate, *Gly* Glycine, *GPC* Glycerophosphocholine, *Ileu* Isoleucine, *Lac* Lactate, *Leu* Leucine, *Lys* Lysine, *PC* Phosphocholine, *PCr* Phosphocreatine, *Phe* Phenylalanine, *Tyr* Tyrosine, *Val* Valine

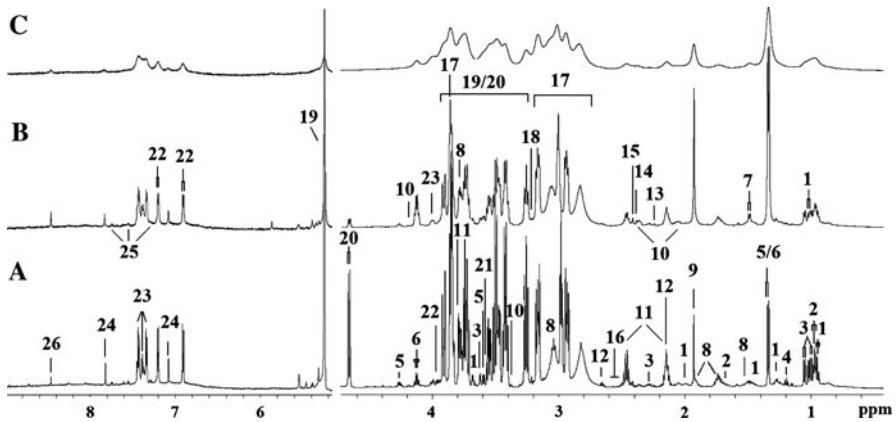

Fig. 2 A series of 600 MHz ^{1}H-NOESY NMR spectra (δ0.5–4.7, δ5.2–9.0) of cell growth medium following the treatment of various doses of USPIO. **a** control, **b** 6 h post-treatment of low-dosage USPIO, and **c** 6 h post-treatment of high-dosage USPIO. The aromatic region was magnified 8 times compared with corresponding aliphatic region for the purpose of clarity. The metabolites numbered were assigned in Table 1

and the resonance assignments (Table 1) were based on the literature (Akhtar et al. 2007; Lamers et al. 2003; Bundy et al. 2006; Miccheli et al. 2006; Bailey et al. 2003), the in-house NMR database and further confirmed with analysis of the 2D NMR spectroscopy (COSY, TOCSY, and J-resolved spectra). As shown in Fig. 2, when the medium is exposed to USPIO, relaxation effect of iron results in broadening of signals in the NMR spectra due to shorter T_2 relaxation. Although the metabolites found in these spectra were broadly similar, differences were observable between the treated media with different-dosage USPIO at the same time point. For example, lactate, pyruvate, acetate, and choline have higher intensities and glucose, glutamine have lower intensities in high-dosage USPIO-treated samples than in low-dosage USPIO-treated samples. However, visual comparison of the spectra alone cannot fulfill complete analysis of the large number of samples and the complexity of metabolite composition. Multivariate data analysis was employed to analyze and identify such differences.

The effects of USPIO on macrophages

Principal component analysis revealed clear differences between control and cells dosed with both low-dose and high-dose USPIO (Fig. 3). The data indicate alterations in the biochemical status with respect to incubation time with USPIO, i.e., between control,

Table 1 ^{1}H-NMR data for the metabolites in the cell medium

No.	Metabolites	^{1}H Shift (Multiplicity)	No.	Metabolites	^{1}H Shift (Multiplicity)
1[a]	Isoleucine	0.94(t[b]), 1.01(d), 1.26(m), 1.48(m), 1.98(m), 3.68(d)	14	Pyruvate	2.37(s)
2	Leucine	0.96(t), 1.71(m)	15	Succinate	2.41(s)
3	Valine	0.99(d), 1.04(d), 2.28(m), 3.62(d)	16	Citrate	2.52(d), 2.55(d)
4	Ethanol	1.19(d), 3.67(q)	17	HEPES	2.82(br), 2.94(m), 2.97(t), 3.03(br), 3.16(m), 3.84(t)
5	Threonine	1.33(d), 3.59(d), 4.26(m)	18	Choline	3.21(s)
6	Lactate	1.33(d), 4.12(q)	19	α-Glucose	3.42(t), 3.54(dd), 3.72(t), 3.74(m), 3.84(m), 5.23(d)
7	Alanine	1.48(d)	20	β-Glucose	3.25(dd), 3.41(t), 3.47(m), 3.49(t), 3.90(dd), 4.65(d)
8	Lysine	1.48(m), 1.73(m), 1.91(m), 3.03(t), 3.76(t)	21	Glycine	3.57(s)
9	Acetate	1.92(s)	22	Tyrosine	3.94(m), 6.90(d), 7.19(d)
10	Proline	2.03(m), 2.35(m), 3.38(m), 4.14(m)	23	Phenylalanine	4.00(m), 7.33(d), 7.38(t), 7.43(dd)
11	Glutamine	2.14(m), 2.46(m), 3.77(t)	24	Histidine	7.07(s), 7.82(s)
12	Methionine	2.14(s), 2.65(t)	25	Tryptophan	7.29(t), 7.36(s), 7.55(d), 7.74(d)
13	Acetone	2.23(s)	26	Formate	8.46(s)

[a] The numbering system is the same as used in Fig. 2

[b] Multiplicity: *s* singlet, *d* doublet, *t* triplet, *q* quartet, *dd* doublet of doublets, *m* multiplet

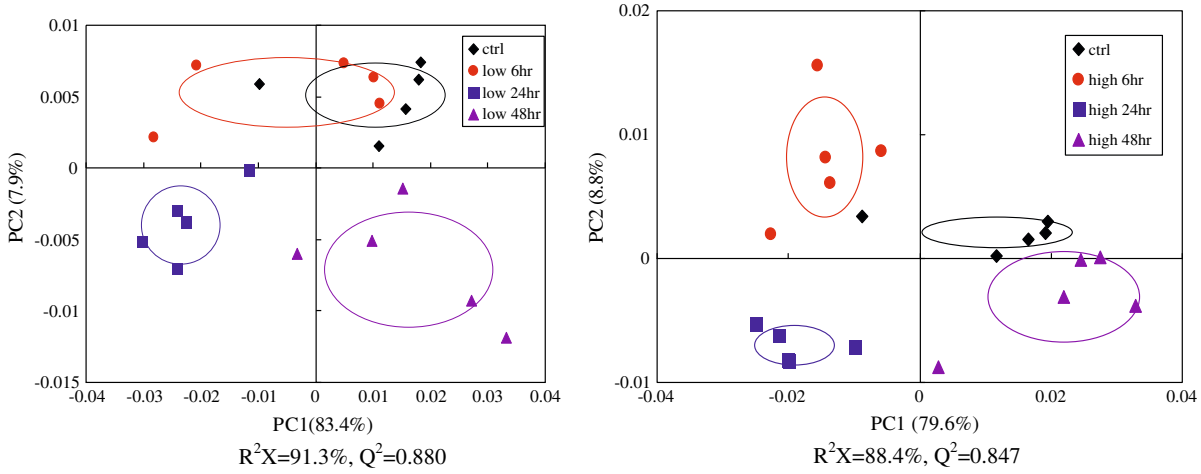

Fig. 3 PCA scores plot based on the ^{1}H-HRMAS NMR spectra of macrophages at various time points following the treatment of low-dosage (*left*) and high-dosage (*right*) USPIO. Control group (*diamonds*), 6 h group (*dots*), 24 h group (*squares*), and 48 h group (*triangles*) post-treatment of USPIO. The center of each ellipse indicates the mean, and the margin indicates one standard deviation

6 h post-dose, 24 h post-dose, and 48 h post-dose samples. The metabolic profiles of low-dose group and high-dose group are quite similar; however, some subtle differences were displayed in the PCA scores plots. Such differences in metabolites can be seen from the PCA scores plots (Fig. 4) in a dose-dependent manner. Following exposure, a significant change in metabolite profile could be observed for

24 h post-treatment, between treatments with either low-dosage or high-dosage of USPIO. However, no obvious difference was displayed between high-dose and low-dose samples for 6 h and 48 h post-treatment (Fig. 4). It was also noted that the greatest metabolic responses occurred at 24 h (Fig. 3), indicating that the first 24 h is an important period for the phagocytic activity of macrophages for USPIO. The profile of 48-h group is similar to the controls, which is illustrated more clearly in the PCA scores plots in the high-dosage group. Dextran groups play a major role in the in vitro and in vivo stability and biocompatibility (Shen et al. 1993; Bulte et al. 1993; Raynal et al. 2004; Nune et al. 2009) and ensure the integrity of USPIO particles, which was evidently reported in previous in vivo studies (Pouliquen et al. 1991; Arbad et al. 2005). The similarity between metabolic profiles of control and 48-h group probably indicates that macrophages undergo a process of phagocytosing and releasing USPIO during 48 h. The cellular metabonomic recovery can also be seen to some degree though not complete.

During the experiments, no obvious cell death was found by Trypan blue staining and microscopic method. The control and low-dosed cells were in a comparatively stable condition according to the growth curve of the macrophages; however, high-dosage USPIO inhibited the growth of macrophages ($p < 0.05$) at 24 and 48 h after the start of the experiment compared with the controls (data not shown). In fact, a maximal iron oxide uptake of up to 50 pg Fe/cell can be obtained by monocytes without impairment of cell viability (Metz et al. 2004); however, the high dosage is only about 0.03 pg Fe/cell in our study, which assures that cell lysis will only be a minor effect.

The effects of USPIO on culture media

The principal component analysis was also performed on NMR data of culture media of macrophages treated with USPIO and compared to control medium (Fig. 5). The first two principal components (PC1 and PC2) explained variations at 93 and 97% for the low- and high-dose samples, respectively. A good quality and predictability ($R^2X = 99.4$, 98.9, and 97.3%, $Q^2 = 0.998$, 0.978, and 0.946 for 6, 24, and 48 h post-treatment, respectively) of PCA model was also obtained when the NMR data were compared between the culture media for various doses. The scores plot showed marked difference between the media treated with low- and high-dose USPIO (Fig. 6).

It can be seen that the culture media samples in the control group are biochemically similar to each other. After USPIO exposure, the samples diverged biochemically with respect to each other, with larger standard deviations (Fig. 5). The effects of the USPIO exposure on the cellular metabolic profiles were greater than the differences by natural divergence. Such a metabolic effect may be attributed to different metabolic response (individual difference) of the macrophages to USPIO exposure. In contrast, the individual difference of macrophages can also be observed in the response to the effects of USPIO from the different metabolic profile in intra-groups (Fig. 3).

Multivariate analyses of macrophage metabonome and medium composition

To get an insight into the types of metabolites responsible for the separation between different cell groups, their loadings plots with correlation coefficients were obtained by using the orthogonal projection to latent structure with discriminant analysis (OPLS-DA), respectively. Figure 4 shows OPLS-DA loadings plot from low- and high-dosed groups at 6, 24, and 24 h post-treatment with USPIO, respectively. Over 6 h, the quiescent cells do not induce metabolic changes, thus the metabolic changes seen at 6 h post-treatment must be as a consequence of exposure to USPIO. Accordingly, the OPLS-DA analysis of the NMR data derived from control and 6 h post-dosed groups was also performed (Fig. 4). The relative changes in metabolites with significant correlation coefficients are tabulated in Table 2 with major discriminating factor between groups, thus providing the biochemical alterations in macrophages following the incubation with USPIO.

The metabolites that had the most influence on the discrimination between control and dosed groups were in the profile of lipids, in which triglyceride was substantially reduced following 6 h of treatment, i.e., it had a large negative value in Fig. 4 and Table 2. The main biological functions of lipids include energy storage and as structural components of cell membranes (McArdle et al. 2001). It is likely that in

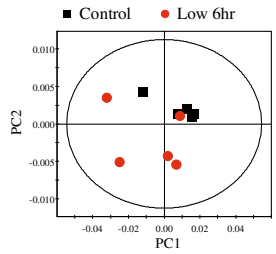

$R^2X=93.9\%$, $Q^2=0.887$

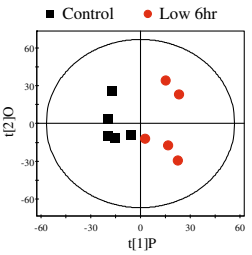

$R^2X=62.4\%$, $Q^2=0.499$

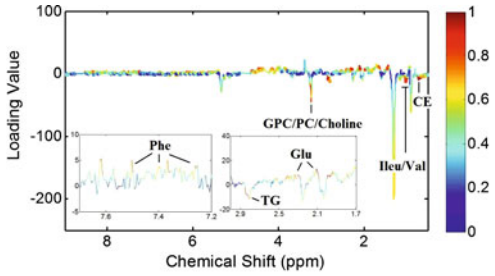

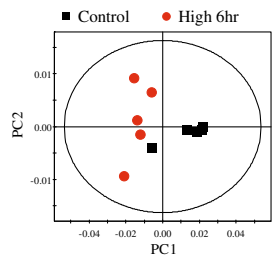

$R^2X=89.1\%$, $Q^2=0.775$

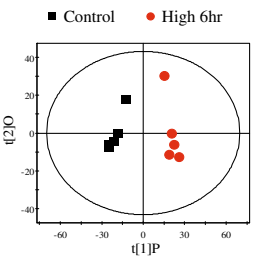

$R^2X=51.1\%$, $Q^2=0.770$

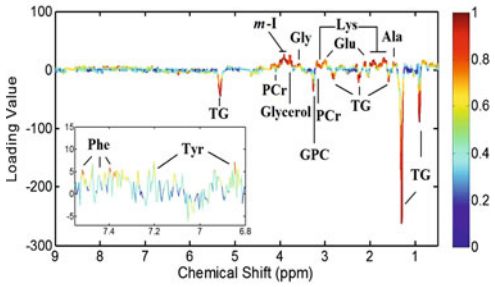

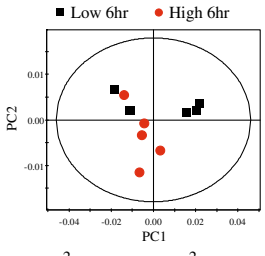

$R^2X=84.9\%$, $Q^2=0.719$

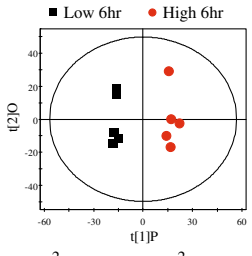

$R^2X=40.8\%$, $Q^2=0.606$

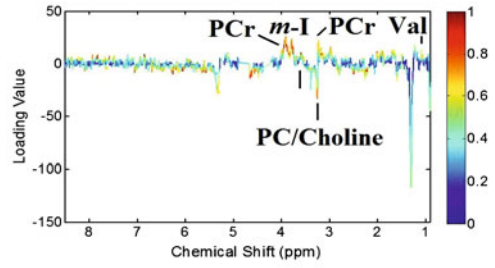

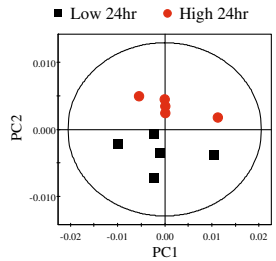

$R^2X=72.7\%$, $Q^2=0.475$

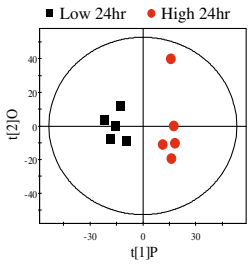

$R^2X=41.1\%$, $Q^2=0.623$

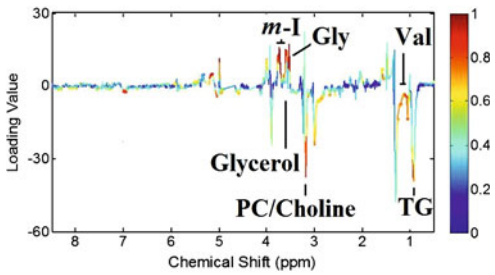

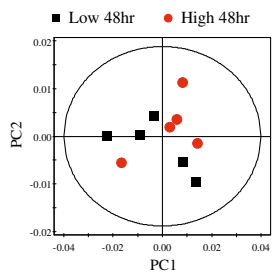

$R^2X=85.4\%$, $Q^2=0.667$

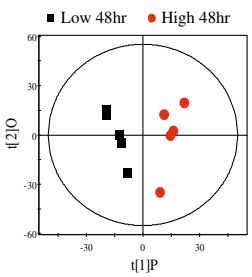

$R^2X=51.6\%$, $Q^2=-0.207$

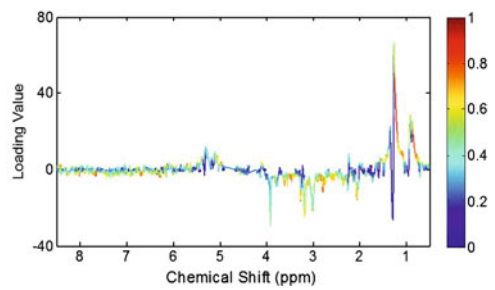

◀ **Fig. 4** PCA scores plots (*left*), OPLS-DA scores (*middle*), and corresponding coefficient plots (*right*) derived from the ^{1}H-HRMAS NMR spectra of macrophages obtained from different groups. The color map shows the significance of metabolite variations between the two classes. Peaks in the positive direction indicate metabolites that are more abundant in the high-dosage USPIO-treated cells or the cells 6 h post-treatment with USPIO than in the low-dosage USPIO-treated cells or pretreated cells. Consequently, metabolites that are more abundant in the pretreated cells or the low-dosage USPIO treated cells are presented as peaks in the negative direction. Keys: *Ala* alanine, *CE* cholesterol, *Glu* glutamate *Gly* glycine, *GPC* glycerophosphocholine, *Ileu* isoleucine, *Lys* lysine, *m-I* *myo*-inositol, *PC* phosphocholine, *PCr* phosphocreatine, *Phe* phenylalanine, *TG* triglyceride, *Tyr* tyrosine, *Val* valine

the early stage (within 24 h post-USPIO treatment), triglycerides are broken down in mitochondria via beta-oxidation to generate acetyl-CoA, and later, fatty acid biosynthesis takes place in the cytoplasm, using acetyl-CoA (derived from carbohydrates, amino acids, or fatty acids) as the precursor (Sychrová 2004). The fatty acids may subsequently be converted to triacylglycerols.

The incubation with USPIO also led to elevation of tyrosine, phenylalanine, lysine, glycine, glutamate, phosphocreatine, *myo*-inositol, and glycerol accompanied with level decreases in valine, isoleucine, and choline metabolites including GPC (glycerophosphocholine), phosphocholine, and choline. As the main components of biological membranes, the concentrations of glycerophospholipids, inositol, GPC/PC, glycerol, and choline are associated with the structural components of cell membranes (Griffin et al. 2001). The decrease of choline containing metabolites in the cells and their increase in the medium are probably associated with cell membrane modification of macrophages. Higher concentration of *myo*-inositol and glycerol in 24 h post-treatment for high dose compared to low dose indicates that modification of cell membrane occurs at an earlier stage. Higher dose of USPIO induced a greater effect on the macrophage metabonome. However, these differences were not significant compared to corresponding metabolites related to dose–effects; the same was observed at 48 h post-treatment (Fig. 4 and Table 2). It implies that USPIO was recycled, being phagocytosed and released by macrophages within 24 h.

Further analyses of NMR data from culture media using PLS-DA showed a clear differentiation in dosage of USPIO with the values of R^2X and Q^2 indicating the validity of the model, where the metabolites had a significant contribution to the dose classification ($|r| > 0.811$) (Fig. 6 and Table 3).

Cells consumed the glucose and essential amino acid such as valine, methionine, and lysine from the DMEM and released metabolic by-products such as lactate and acetate, where an obvious dose–effect relationship was seen. Glucose and amino acid utilization, with the production of lactate and alanine, are in agreement to the tumor cell metabonome, which is characterized by high glycolytic capacities under strong variations in energy and glucose supply (Mazurek and Eigenbroadt 2003). Lactate release is closely correlated with the variance of the glucose utilization due to the mainly cytosolic pyruvate production from glycolysis. Furthermore, alanine is released as an energy source from the alanine–glucose cycle after the formation of pyruvate from

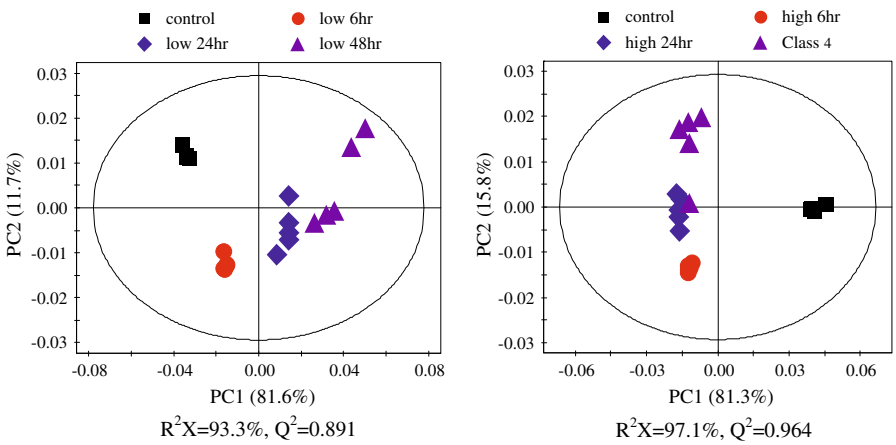

Fig. 5 PCA scores plot based on the ^{1}H-NMR spectra of cell growth media from at various time points following the treatment of low-dosage (*left*) and high-dosage (*right*) USPIO. Control group, *squares*; 6h group, *dots*; 24 h group, *diamonds*; 48 h group, *triangles* post-treatment of USPIO

glycolysis. On the other hand, after exposure to higher-dosage USPIO, cells excrete more intermediate citrate and succinate via citric acid cycle (TCA cycle) into the extracellular medium. The presence of these metabolites suggests the higher-dosage USPIO induced more extensive glycolysis in both anaerobic and aerobic pathway for macrophages.

It may be concluded that the differential response to exposure to USPIO for the first 24 h, in both cell metabonome and medium components, was a key time point over which period the macrophages both phagocytose and release of USPIO; this biological effects may not be the case for all cell-types. This hypothesis is supported by

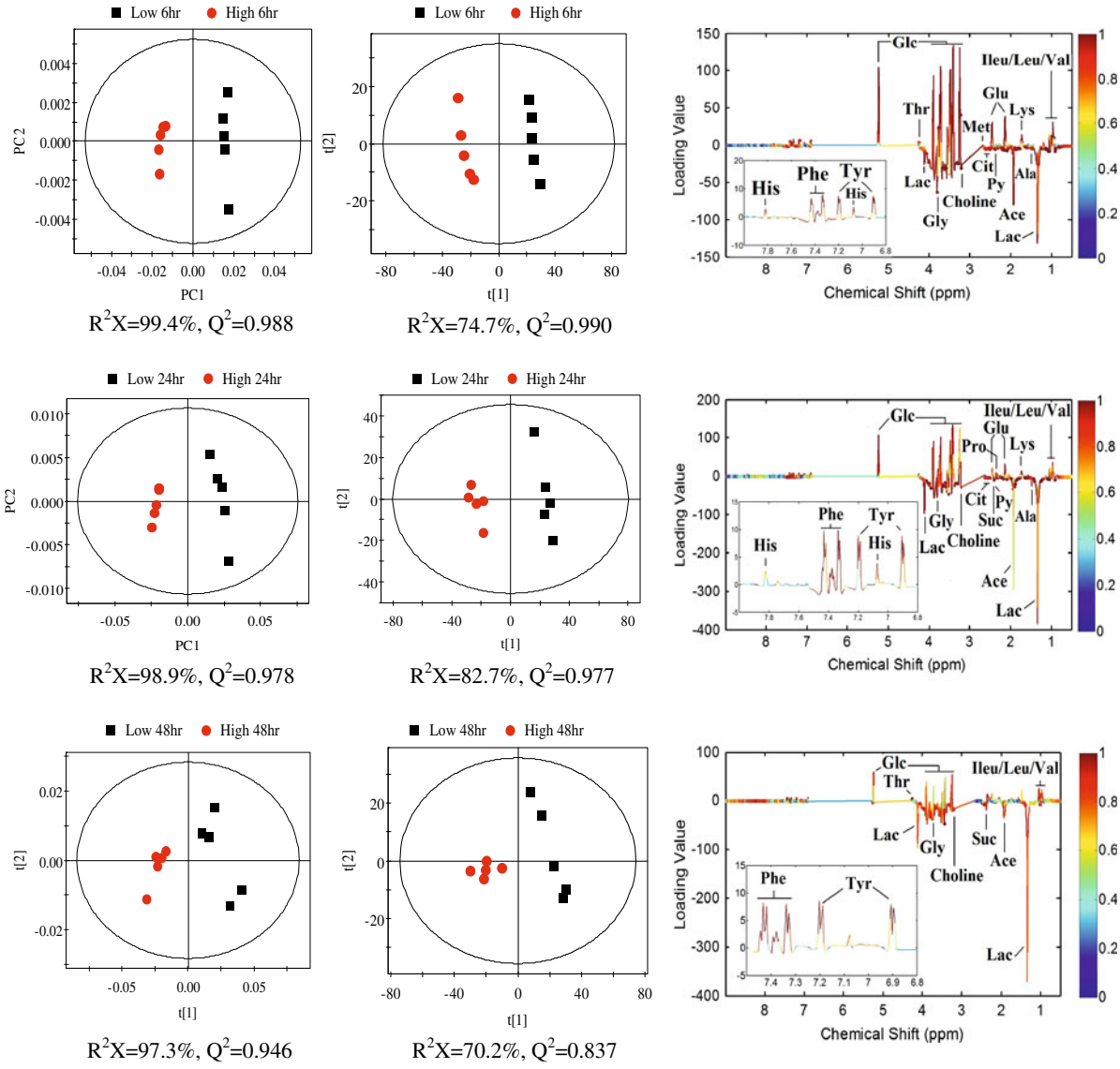

Fig. 6 PCA scores plots (*left*), PLS-DA scores (*middle*), and corresponding coefficient plots (*right*) derived from the ^{1}H NOESY NMR spectra of incubation medium obtained from different groups. The color map shows the significance of metabolite variations between the two classes. Peaks in the positive direction indicate metabolites that are more abundant in the low-dosage medium than in the high-dosage medium. Consequently, metabolites that are more abundant in the high-dosage medium are presented as peaks in the negative direction. Keys: *Ace* acetate, *Ala* alanine, *Cit* citrate, *Glc* Glucose, *Glu* glutamine, *Gly* glycine, *His* histidine, *Ileu* isoleucine, *Lac* lactate, *Leu* leucine, *Lys* lysine, *Met* methonine, *Phe* phenylalanine, *Pro* proline, *Py* Pyruvate, *Suc* succinate, *Thr* threonine, *Tyr* tyrosine, *Val* valine

Table 2 OPLS-DA Coefficients derived from the NMR data of metabolites in each group cells treated with different-dosage USPIO

Metabolites	r[a]				
	C–L6[b]	C–H6	L6–H6	L24–H24	L48–H48
Valine: 1.04(d[c]); 0.99(d)	−0.865	–	0.817	–	–
Tyrosine: 7.20(d); 6.91(d)	–	0.816	–	–	–
Triglyceride, CH_3–(CH_2)$_n$–: 1.29(br)	–	−0.929	–	–	–
Triglyceride, CH_3–(CH_2)$_n$–: 0.89(br)	–	−0.940	–	−0.872	–
Triglyceride, –CH_2–CH_2–C=O: 2.26(br)	–	−0.951	–	–	–
Triglyceride, –CH_2–CH_2–C=O: 1.59(br)	–	−0.891	–	–	–
Triglyceride, –CH_2–CH=CH–: 2.03(br)	–	–	–	–	–
Phosphocreatine: 3.93(s), 3.04(s)	–	0.970	0.845	–	–
Phenylalanine: 7.43(dd); 7.37(t); 7.32(d)	0.866	0.873	–	–	–
myo-inositol: 3.92(t); 3.62(dd); 3.25(t)	–	0.979	0.817	0.931	–
Lysine: 3.76(t); 3.03(t); 1.91(m); 1.72(m)	–	0.952	–	–	–
Triglyceride, –CH=CH–: 5.33(br)	–	−0.932	–	–	–
Triglyceride, =CH–CH_2–CH=: 2.81(br)	−0.933	−0.969	–	–	–
Isoleucine: 1.01(d); 0.94(t)	−0.921	–	–	−0.816	–
Glycine: 3.57(s)	–	0.940	0.821	0.889	–
GPC: 3.23(s)	−0.836	−0.880	–	–	–
Glycerol: 3.68(m)	–	0.882	–	0.912	–
Glutamate: 3.77(t); 2.36(m); 2.10(m)	0.910	0.943	–	–	–
PC/Choline: 3.20(s)	−0.836	–	−0.842	−0.908	–
Alanine: 1.48(d)	–	0.890	–	–	–

[a] Correlation coefficients, positive and negative signs indicate positive and negative correlation in the concentrations, respectively. The correlation coefficient of $|r| > 0.811$ was used as the cutoff value for the statistical significance based on the discrimination significance at the level of $p = 0.05$ and df (degree of freedom) $= 4$. ''−'' means the correlation coefficient $|r|$ is less than 0.811

[b] *C* control, *L6 (L24, L48)* 6 h (24 h, 48 h) post-treatment with low-dosage USPIO, *H6 (H24, H48)* 6 h (24 h, 48 h) post-treatment with high-dosage USPIO

[c] Multiplicity: *s* singlet, *d* doublet, *t* triplet, *q* quartet, *dd* doublet of doublets, *m* multiplet, *br* broad resonance

the pharmacokinetic, distribution and degradation studies of iron oxide nanoparticles in the animal models, in which most of iron oxide nanoparticles were usually phagocytosed in hours (Pouliquen et al. 1991) and transferred to liver and spleen from mononuclear phagocytic system within 24 h following single intravenous administration (Okon et al. 1994; Briley-Saebo et al. 2004). In the high-dosage group, the more extensive utilization of glucose and amino acids, especially tryptophan, threonine, proline, isoleucine, and glycine, were observed (Figs. 4 and 6, and Tables 2, 3). Following acquisition and analysis of NMR data on intact macrophage and their culture media, it is clear that the respective metabonomes are dependent on the dose of USPIO, which are dominated by metabolites involved in energy consumption and membrane components.

Conclusions

In summary, a metabonomic study presents a powerful and relatively simple tool for investigating cellular metabolic phenotypes allowing the evaluation of biochemical changes due to exposure to nanoparticles. This study has demonstrated that USPIO treatment of murine RAW264.7 macrophage-like cell line results in biochemical changes relating to energy production and the TCA cycle. Multivariate data analysis of ^{1}H-NMR spectra showed clear discrimination between high- and

Table 3 PLS-DA Coefficients derived from the NMR data of metabolites in each group medium treated with different-dosage USPIO

Metabolites	r[a]		
	L6–H6[b]	L24–H24	L48–H48
β-Glucose	0.997	0.990	0.926
α-Glucose	0.996	0.991	0.928
Valine	0.996	0.981	0.978
Tyrosine	0.907	0.992	0.974
Tryptophan	0.989	0.800	0.988
Threonine	0.852	0.966	0.988
Succinate	–	−0.938	−0.888
Pyruvate	−0.972	−0.978	−0.880
Proline	–	0.921	0.956
Phenylalanine	0.997	0.995	0.990
Methionine	0.990	0.989	–
Lysine	0.983	0.976	–
Leucine	0.997	0.987	0.927
Lactate	−0.950	−0.944	−0.895
Isoleucine	0.991	0.956	0.903
Histidine	0.973	0.895	–
Glycine	−0.976	−0.987	−0.995
Glutamine	0.995	0.983	–
Citrate	−0.975	−0.963	–
Choline	−0.996	−0.996	−0.900
Alanine	−0.956	−0.922	–
Acetate	−0.988	−0.919	−0.905

[a] Correlation coefficients, positive and negative signs indicate positive and negative correlation in the concentrations, respectively. The correlation coefficient of $|r| > 0.811$ was used as the cutoff value for the statistical significance based on the discrimination significance at the level of $p = 0.05$ and df (degree of freedom) = 4. ''−'' means the correlation coefficient $|r|$ is less than 0.811

[b] *L6 (L24, L48)* 6 h (24 h, 48 h) post-treatment with low-dosage USPIO, *H6 (H24, H48)* 6 h (24 h, 48 h) post-treatment with high-dosage USPIO

low-dose groups, demonstrating the metabolic effects of USPIO with increased expression of glycerophospholipids, tyrosine, phenylalanine, lysine, glycine, glutamate, glutamine together with decrease in triglyceride, and essential amino acids such as valine, isoleucine, and choline-like metabolites for the cell metabonome. A decrease of glucose and amino acids and an increase of end-products and intermediates such as pyruvate, lactate, acetate, citrate, and succinate during both anaerobic and aerobic glycolytic processes in the culture medium have also been observed. Current data indicated that the metabolic features of macrophage appeared to be present for the key time point of phagocytosis and release of USPIO together with the information of cell membrane modification. NMR spectroscopy, in combination with multivariate data analysis, seems to be a suitable technique allowing the simultaneous quantification of many metabolites without a prior knowledge of the involved biochemical pathway and leading to the identification of a specific metabolic fingerprint.

Acknowledgments We acknowledge the financial supports from the National Natural Science Foundation of China (20605025, 20825520, and 20921004), and the Chinese Academy of Sciences. We also thank Dr. Hang Zhu, Wuhan Institute of Physics and Mathematics, for modifying the matlab scripts used for color-coded loading plots.

References

Akhtar SV, Singh RK, Jadegoud Y, Dhole TN, Ayyagari A, Gowda GAN (2007) In vitro ^{1}H NMR studies of RD human cell infection with Echovirus 11. NMR Biomed 20:422–428

Anzai Y, Piccoli CW, Outwater EK, Stanford W, Bluemke DA, Nurenberg P, Saini S, Maravilla KR, Feldman DE, Schmiedl UP, Brunberg JA, Francis IR, Harms SE, Som PM, Tempany CM (2003) Evaluation of neck and body metastases to nodes with Ferumoxtran 10-enhanced MR imaging: phase III safety and efficacy study. Radiology 228:777–788

Arbad AS, Wilson LB, Ashari P, Jordan EK, Lewis BK, Frank JA (2005) A model of lysosomal metabolism of dextran coated superparamagnetic iron oxide (SPIO) nanoparticles: implications for cellular magnetic resonance imaging. NMR Biomed 18:383–389

Bailey NJC, Oven M, Holmes E, Nicholson JK, Zenk MH (2003) Metabolomic analysis of the consequences of cadmium exposure in silence cucubalus cell cultures via ^{1}H NMR spectroscopy and chemometrics. Phytochemistry 62:851–858

Bollard ME, Garrod S, Holmes E, Lindon JC, Humpfer E, Spraul M, Nicholson JK (2000) High-resolution (1)H and (1)H-(13)C magic angle spinning NMR spectroscopy of rat liver. Magn Reson Med 44:201–207

Briley-Saebo K, Bjørnerud A, Grant D, Ahlstrom H, Berg T, Kindberg GM (2004) Hepatic cellular distribution and degradation of iron oxide nanoparticles following single intravenous injection in rats: implications for magnetic resonance imaging. Cell Tissue Res 316:315–323

Bulte JWM, Ma LD, Magin RL, Kamman RL, Hulstraert CE, Go KG, The TH, de Leij L (1993) Selective MR imaging of labeled human peripheral blood mononuclear cells by liposomes mediated incorporation of dextran-magnetic particles. Magn Reson Med 29:32–37

Bundy JG, Lenz EM, Bailey NJ, Gavaghan CL, Svendsen C, Spurgeon D, Hankard PK, Osborn D, Weeks JM, Trauger SA, Speir P, Sanders I, Lindon JC, Nicholoson JK, Tang HR (2002) Metabonomic assessment of toxicity of 4-fluoroaniline, 3, 5-difluoroaniline and 2-fluoro-4-methylaniline to the earthworm eisenia veneta (ROSA): identification of new endogenous biomarkers. Environ Toxicol Chem 21:1966–1972

Bundy JG, Iyer NG, Gentile MS, Hu DE, Kettunen M, Maia AT, Thorne NP, Brenton JD, Caldas C, Brindle KM (2006) Metabolic consequences of p300 gene deletion in human colon cancer cells. Cancer Res 66:7606–7614

Coen M, Wilson ID, Nicholson JK, Tang HR, Lindon JC (2004) Probing molecular dynamics in chromatographic systems using high-resolution H-1 magic-angle-spinning NMR spectroscopy: interaction between p-xylene and c18-bonded silica. Anal Chem 76:3023–3028

Daldrup-Link HE, Rudelius M, Oostendorp RAJ, Settles M, Piontek G, Metz S, Rosenbrock H, Keller U, Heinzmann U, Rummeny EJ, Schlegel J, Link TM (2003) Targeting of hematopoietic progenitor cells with MR contrast agents. Radiology 228:760–767

Dousset V, Ballarino L, Delalande C, Coussemacq M, Canioni P, Petry KG, Caillé JM (1999) Comparison of ultrasmall particles of iron oxide (USPIO)-enhanced T2-weighted, conventional T2-weighted, and gadolinium-enhanced T1-weighted MR images in rats with experimental autoimmune encephalomyelitis. Am J Neuroradiol 20:223–227

Duarte IF, Marques J, Ladeirinha AF, Rocha C, Lamego I, Calheiros R, Silva TM, Marques MPM, Melo JB, Carreira IM, Gil AM (2009) Analytical approaches toward successful human cell metabolome studies by NMR spectroscopy. Anal Chem 81:5023–5032

Fabene PF, Marzola P, Sbarbati A, Bentivoglio M (2003) Magnetic resonance imaging of changes elicited by status epilepticus in the rat brain: diffusion-weighted and T2-weighted images, regional blood volume maps, and direct correlation with tissue and cell damage. NeuroImage 18: 375–389

Griffin JL, Mann CJ, Scott J, Shoulders CC, Nicholson JK (2001) Choline containing metabolites during cell transfection: an insight into magnetic resonance spectroscopy detectable changes. FEBS Lett 509:263–266

Griffin JL, Bollard M, Nicholson JK, Bhakoo K (2002) Spectral profiles of cultured neuronal and glial cells derived from HRMAS H-1 NMR spectroscopy. NMR Biomed 15:375–384

Griffin JL, Pole JCM, Nicholson JK, Carmichael PL (2003) Cellular environment of metabolites and a metabonomic study of tamoxifen in endometrial cells using gradient high resolution magic angle spinning ^{1}H NMR spectroscopy. Biochim Biophys Acta 1619:151–158

Halbreich A, Groman EV, Raison D, Bounchaud C, Paturance S (2002) Damage to the protein synthesizing apparatus in mouse liver in vivo by magnetocytolysis in the presence of hepatospecific magnetic nanoparticles. J Magn Mater 248:276–285

Josephson L, Tung CH, Moore A, Weissleder R (1999) High-efficiency intracellular magnetic labeling with novel superparamagnetic-tat peptide conjugates. Bioconjug Chem 10:186–191

Kell DB, Brown M, Davey HM, Dunn WB, Spasic I, Oliver SG (2005) Metabolic footprinting and systems biology: the medium is the message. Nat Rev Microbiol 3:557–565

Kresse M, Wagner S, Pfefferer D, Lawaczeck R, Elste V, Semmler W (2005) Targeting of ultrasmall superparamagnetic iron oxide (USPIO) particles to tumor cells in vivo by using transferring receptor pathways. Magn Reson Med 40:236–242

LaConte L, Nitin N, Bao G (2005) Magnetic nanoparticle probes. Nanotoday 32–38

Lamers RJAN, Wessels ECHH, van de Sandt JJM, Venema K, Schaafsma G, van der Greef J, van Nesselrooij JHJ (2003) A pilot study to investigate effects of inulin on Caco-2 cells through in vitro metabolic fingerprinting. J Nutr 133:3080–3084

Li JV, Holmes E, Saric J, Keiser J, Dirnhofer S, Ultzinger J, Wang YL (2009) Metabolic profiling of a schistosoma mansoni infection in mouse tissues using magic angle spinning-nuclear magnetic resonance spectroscopy. Int J Parasitol 39:547–558

Mazurek S, Eigenbroadt E (2003) The tumor metabolome. Anticancer Res 23:1149–1154

McArdle WD, Katch FI, Katch VL (2001) Exercise physiology: energy, nutrition and human performance, Chapter 4, 5th edn. Lippincott Williams & Wilkins ISBN 07817 25445

Metz S, Bonaterra G, Rudelius M, Settles M, Rummeny EJ, Daldrup-Link HE (2004) Capacity of human monocytes to phagocytose approved iron oxide MR contrast agents in vitro. Eur Radiol 14:1851–1858

Metz S, Lohr S, Settles M, Beer A, Woertler K, Rummeny EJ, Daldrup-Link HE (2006) Ferumoxtran-10-enhanced MR imaging of the bone marrow before and after conditioning therapy in patients with non-Hodgkin lymphomas. Eur Radiol 16:598–607

Miccheli AT, Miccheli A, Di Clemente R, Valerio M, Coluccia P, Bizzari M, Conti F (2006) NMR-based metabolic profiling of human hepatoma cells in relation to cell growth by culture media analysis. Biochim Biophys Acta 1721:98–106

Nicholson JK, Lindon JC, Holmes E (1999) 'Metabonomics': understanding the metabolic responses of living systems to pathophysiological stimuli via multivariate statistical analysis of biological NMR spectroscopic data. Xenobiotica 29:1181–1189

Nune SK, Gunda P, Thallapally P, Lin YY, Laird Forrest M, Berkland CJ (2009) Expert opinion on drug delivery. Expert Opin Drug Deliv 6:1175–1194

Okon E, Pouliquen D, Okon P, Kovaleva ZV, Stepanova TP, Lavit SG, Kudryavtsev BN, Jallet P (1994) Biodegradation of magnetite dextran nanoparticles in the rat. A histologic and biophysical study. Lab Invest 71:895–903

Pouliquen D, Le Jeune JJ, Perdrisot R, Ermias A, Jallet P (1991) Iron oxide nanoparticles for use as an MRI contrast agent: pharmacokinetics and metabolism. Magn Reson Imaging 9:275–283

Raynal I, Prigent P, Peyramaure S, Najid A, Rebuzzi C, Corot C (2004) Macrophage endocytosis of superparamagnetic iron oxide nanoparticles—mechanisms and comparison of ferumoxides and ferumoxtran-10. Invest Radiol 39:56–63

Saini S, Stark DD, Hahn PF, Wittenberg J, Brady TJ, Ferrucci JT (1987) Ferrite particles: a superparamagnetic MR contrast agent for the reticuloendothelial system. Radiology 162:211–216

Saksena MA, Saokar A, Harisinghani MG (2006) Lymphotropic nanoparticle enhanced MR imaging (LNMRI) technique for lymph node imaging. Eur J Radiol 58:367–374

Shen T, Weissleder R, Papisov M, Bogdanov A, Brady TJ (1993) Monocrystalline iron oxide nanocompounds (MION): physicochemical properties. Magn Reson Med 29:599–604

Simpson MJ, McKelvie JR (2009) Environmental metabolomics: new insights into earthworm ecotoxicity and contaminant bioavailability in soil. Anal Bioanal Chem 394: 137–149

Sychrová H (2004) Yeast as a model organism to study transport and homeostasis of alkali metal cations. Physiol Res 53(Suppl. 1):S91–S98

Tang HR, Wang YL (2006) Metabonomics: a revolution in progress. Prog Biochem Biophys 33:401–417

Wang YL, Holmes E, Nicholson JK, Cloarec O, Chollet J, Tanner M, Singer BH, Utzinger J (2004) Metabonomic investigations in mice infected with schistosoma mansoni: an approach for biomarker identification. Proc Natl Acad Sci USA 101:12676–12681

Wang YL, Tang HR, Holmes E, Lindon JC, Turini ME, Sprenger N, Bergonzelli G, Fay LB, Kochhar S, Nicholson JK (2005) Biochemical characterization of rat intestine development using high-resolution magic-angle-spinning H NMR spectroscopy and multivariate data analysis. J Proteome Res 4:1324–1329

Wang YL, Holmes E, Tang HR, Lindon JC, Sprenger N, Turini ME, Bergonzelli G, Fay LB, Kochhar S, Nicholson JK (2006) Experimental metabonomic model of dietary variation and stress interactions. J Proteome Res 5:1535–1542

Wang YL, Holmes E, Comelli EM, Fotopoulos G, Dorta G, Tang HR, Rantalainen MJ, Lindon JC, Corthsy-Theulaz IE, Fay LB, Kochhar S, Nicholson JK (2007) Topographical variation in metabolic signatures of human gastrointestinal biopsies revealed by high-resolution magic-angle spinning H NMR spectroscopy. J Proteome Res 6:3944–3951

Wang YL, Cloarec O, Tang HR, Lindon JC, Noimes E, Kochhar S, Nicholson JK (2008) Magic angle spinning NMR and H-1-P-31 heteronuclear statistical total correlation spectroscopy of intact human gut biopsies. Anal Chem 80:1058–1066

Wei L, Liao PQ, Wu HF, Li XJ, Pei FK, Li WS, Wu YJ (2009) Metabolic profiling studies on the toxicological effects of realgar in rats by H-1 NMR spectroscopy. Toxicol Appl Pharm 234:314–325

Weishaupt D, Hetzer FH, Ruehm SG, Patak MA, Schmidt M, Debatin JF (2000) Three-dimensional contrast-enhanced MRI using an intravascular contrast agent for detection of traumatic intra-abdominal hemorrhage and abdominal parenchymal injuries: an experimental study. Eur Radiol 10:1958–1964

Weissleder R, Cheng HC, Bogdanova A Jr, Bogdanov A (1997) Magnetically labeled cells can be detected by MR imaging. J Magn Reson Imaging 7:258–263

Yang MS, Yu LC, Gupta RC (2005) Analysis of multiple metabolomic subset in vitro: methodological considerations. Toxicol Mech Methods 15:29–32

Yang Y, Li C, Nie X, Feng X, Chen W, Yue Y, Tang H, Deng F (2007) Metabonomic studies of human hepatocellular carcinoma using high-resolution magic-angle spinning ^{1}H NMR spectroscopy in conjunction with multivariate data analysis. J Proteome Res 6:2605–2614